

SIMULATION INVESTIGATION OF ROTOR LOADS AND BLADE DEFORMATIONS IN STEADY STATES AND AT BOUNDARIES OF HELICOPTER FLIGHT ENVELOPE

Jarosław Stanisławski

*Institute of Aviation
Krakowska Av. 110/114, 02-256 Warszawa, Poland
tel.: +48 22 846 00 11 ext. 362
e-mail: jaroslaw.stanislawski@ilot.edu.pl*

Abstract

Results of calculation of the helicopter main rotor loads and deformations of rotor blades are presented. The simulations concern level flight states and cases of boundary flight envelope such as wind gust, dive recovery and pull-up manoeuvre. The calculations were performed for data of the three-bladed articulated rotor of light helicopter. The method of analysis assumes modelling the rotor blades as elastic axes with sets of lumped masses of blade segments distributed along radius of blade. The model of deformable blade allows flap, lead-lag and pitch motion of blade including effects of out-of-plane bending, in-plane bending and torsion due to aerodynamic and inertial forces and moments acting on the blade. Equations of motion of rotor blades are solved applying Runge-Kutta method. Parameters of blade motion, according to Galerkin method, are considered as a combination of assumed torsion and bending eigen modes of the rotor blade. The rotor loads, in all considered cases of flight states, are calculated for quasi-steady conditions assuming the constant value of the following parameters: rotor rotational speed, position of the main rotor axis in air and position of swashplate due to rotor axis which defines the collective and cyclic control pitch angle of blades. The results of calculations of rotor loads and blade deflections are presented in form of time-runs and as distributions on rotor disk due to blade elements radial and azimuthal positions. The simulation investigation may help to collect data for prediction the fatigue strength of blade applying results for steady flight states and for definition the extreme loads for boundaries of helicopter flight envelope.

Keywords: *helicopter, rotor loads, blade deformation*

1. Introduction

Knowledge concerning main rotor loads generated within helicopter flight envelope is one of important factors, which influences a design process. The computer codes of rotorcraft analysis such as CAMRAD, FLIGHTLAB or UMARC were developed [1] to enable prediction of rotor loads including effects of complex airflow conditions of rotating blades, inputs of blade pitch control and variable blade deflections. Performed by NASA/Army UH-60A Airloads Program comprised flight tests [2] and wind tunnel research [3, 4], which allow to collect data for verification and comparing results of rotorcraft analysis methods. An estimation of accuracy of the CAMRAD code was investigated comparing measured data of in flight and wind tunnel tests, for several types of helicopters operating at transition and high speed conditions, with results of calculations for isolated rotor models [5]. Further improvement of rotor loads computation comprises application of CFD/CSD coupling (Computational Fluid Dynamics / Computational Structure Dynamics) which combines complex flow physics, nonlinear structural dynamics and geometrical complexity of rotorcraft [6].

In the Institute of Aviation, a simulation method of rotor loads calculation has been developed which was applied during design and tests of the ILX-27 unmanned helicopter [7, 8]. The results of calculations, presented in this article, were obtained for data of the modified version of the three-bladed ILX-27 rotor with increased blade radius. The airfoils of the ILH family, designed in the Institute of Aviation, were applied for the rotor blades. The isolated rotor model was applied to

simulate steady level flight cases with arising speed of helicopter flight. The cases of wind gust, dive recovery and initial phase of pull up were treated as quasi-steady states including constant position of swashplate, pitch angle of rotor shaft axis and constant rotational rotor speed. The time-run plots of rotor thrust, torsion moments of rotor shaft and blade control moments are compared for the several states of the helicopter flight envelope. The comparison of rotor blade behaviour and flow conditions is shown in form of rotor disk distributions of blade deflections and blade cross-section angles of attack.

2. Model of rotor

The model of a helicopter rotor includes blades with rotor head arms. The real structure of blades and arms are replaced by the elastic axes with sets of lumped masses distributed along the radius of blades (Fig. 1). The blades are divided into segments, which are substituted by lumped masses represent the inertial features of the blades. The elastic axes are divided into sectors, located between cross-sections of the neighbouring lumped masses. The blade bending and torsion stiffness are assigned to sectors of the elastic axes.

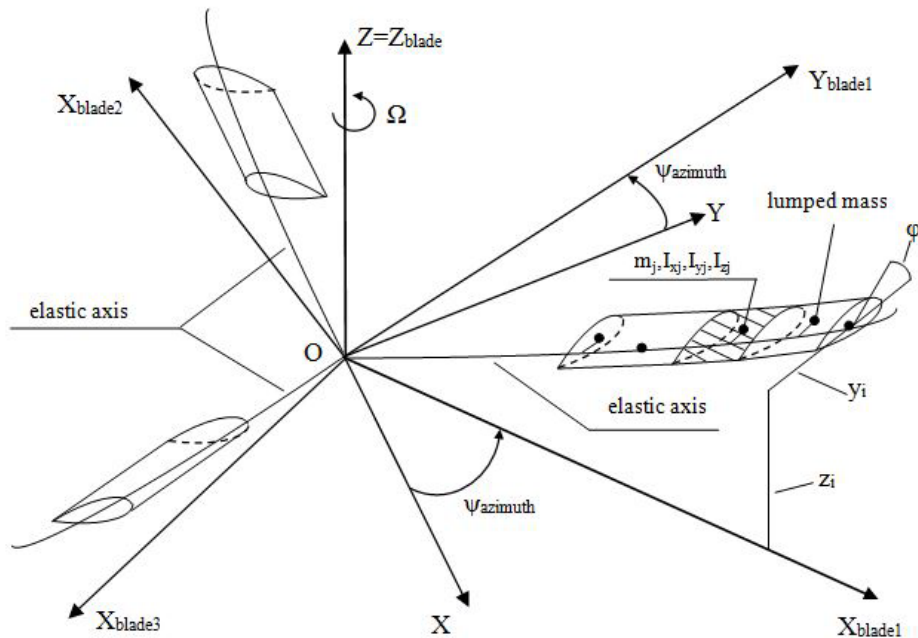


Fig. 1. Physical model of helicopter rotor includes blade elastic axes with sets of lumped masses

The following assumptions are applied to define the physical model of rotor:

- inertial, stiffness and geometrical features of all rotor blades are the same,
- lumped masses represent the inertial features of the corresponding blade segments (mass m_i , inertial moments I_{xi}, I_{yi}, I_{zi}),
- sectors of blade elastic axis connect the blade cross-sections including the lumped masses,
- blade elastic axis can be twisted and bent in the rotor revolution and thrust planes,
- the blades are connected with rotor head by articulated joints with allowed coupling of flap and pitch blade motion,
- the blade pitch axis takes coincident position to the non-deformed blade elastic axis.

The implementation of calculation algorithm includes a multi-blades analysis which allows to compute, at the given time moment, the components of motion and loads for individual blades due to their different azimuth position on the rotor disk. The mathematical model of rotor comprises the equations of motion of the elastic axis, which for deformable blades with continuous distribution of mass and stiffness can be derived as follows:

– for in-plane bending

$$\int_0^R m(x)\ddot{y} dx + \int_0^R \left\{ \frac{d^2}{dx^2} \left[EJ_z \left(\frac{d^2 y}{dx^2} \right) \right] - \frac{d}{dx} \left(N \frac{dy}{dx} \right) + m(x)\Omega^2 y \right\} dx = \int_0^R (F_{Yaero} + F_{YG} + F_{Yiner}) dx, \quad (1)$$

– for out-of-plane bending

$$\int_0^R m(x)\ddot{z} dx + \int_0^R \left\{ \frac{d^2}{dx^2} \left[EJ_y \left(\frac{d^2 z}{dx^2} \right) \right] - \frac{d}{dx} \left(N \frac{dz}{dx} \right) \right\} dx = \int_0^R (F_{Zaero} + F_{ZG} + F_{Ziner}) dx, \quad (2)$$

– for torsion

$$\int_0^R I_X(x)\ddot{\phi} dx + \int_0^R \frac{d}{dx} \left[GJ_X \left(\frac{d\phi}{dx} \right) \right] dx = \int_0^R (M_{Taero} + M_{TG} + M_{Tiner}) dx, \quad (3)$$

where:

y, z, ϕ – deformation of elastic axis respectively in-plane, out-of-plane and torsion,
 EJ_z, EJ_y, GJ_x – stiffness of elastic axis bending in-plane and out-of-plane and torsion,
 Ω – rotational speed of the main rotor,

$N = \int_r^R m(x)\Omega^2 x dx$ – local centrifugal force at cross-section located at distance r from axis of the rotor shaft,

$\frac{d}{dx} \left(N \frac{dy}{dx} \right) + m(x)\Omega^2 y$ – cross-section in-plane load correction due to the centrifugal force,

$\frac{d}{dx} \left(N \frac{dz}{dx} \right)$ – cross-section out-of-plane load correction due to the centrifugal force,

$F_{Yaero}, F_{YG}, F_{Yiner}, F_{Zaero}, F_{ZG}, F_{Ziner}, M_{Taero}, M_{TG}, M_{Tiner}$ – shear forces and torsion moments of aerodynamic, gravitation and inertial loads acting on segment dx of elastic axis.

System of equations (1)-(3) is solved applying Galerkin method, which assumes that the elastic axis parameters of motion are equal to the sum of the considered eigen modes of the rotor blades.

The deflections of the blade elastic axis y, z, ϕ are equal to superposition of modal components:

$$y(x,t) = \sum_{i=1}^I \rho_i(t)y_i(x); \quad z(x,t) = \sum_{j=1}^J \delta_j(t)z_j(x); \quad \phi(x,t) = \sum_{k=1}^K \eta_k(t)\phi_k(x), \quad (4)$$

where:

y_i, z_j, ϕ_k – eigen modes of in-plane, out-of-plane bending and torsion respectively,

ρ_i, δ_j, η_k – time dependent shares of eigen modes, which are determined in computing process,

I, J, K – numbers of considered bending and torsion eigen modes.

According to dependences (4), the equations of blade motion can be converted into sets of equations (5)-(7) related to each considered blade eigen mode:

$$\ddot{\rho}_i + \rho_i p_i^2 = Q_{Y_i}, \quad i = 1, \dots, I, \quad (5)$$

$$\ddot{\delta}_j + \delta_j f_j^2 = Q_{Z_j}, \quad j = 1, \dots, J, \quad (6)$$

$$\ddot{\eta}_k + \eta_k v_k^2 = Q_{\phi_k}, \quad k = 1, \dots, K, \quad (7)$$

where:

p_i^2, f_j^2, v_k^2 – square of eigen mode frequencies for bending in-plane, out-of-plane and torsion,

$Q_{Y_i}, Q_{Z_j}, Q_{\phi_k}$ – generalized forces for each eigen modes of the rotor blade.

The equations of motion (5)-(7) are solved by applying Runge-Kutta method. After determining at a given moment of time the contribution of generalized displacements ρ_i , δ_j , η_k , velocities and accelerations for each eigen mode the resultant parameters of the blade motion can be computed. Repeating the cycle of calculation allows defining deformation of blades and loads of rotor.

Aerodynamic forces acting on segment of blade at given azimuth position on the rotor disk are computed applying the blade element theory. The local angle of attack at blade cross-section depends on control of pitch angle and on temporary conditions of airflow:

$$\alpha = \varphi_o + \varphi_x \cos\Omega t + \varphi_y \sin\Omega t + \varphi_{geom} + \Delta\varphi_{torsion} - \kappa\beta - \text{arc tg}\left(\frac{u_z}{u_x}\right), \quad (8)$$

where:

φ_o – blade collective control angle,

φ_o, φ_o – cyclic control angle due to roll and pitch deflections of the swashplate,

φ_{geom} – blade geometric twist,

$\Delta\varphi_{torsion}$ – torsion deformation,

κ – coefficient of coupling flap and blade pitch,

β – blade flap angle at horizontal hinge of rotor head,

u_z, u_x – components of the cross-section airflow of rotor blade: out-of-plane and in-plane.

3. Results of simulation

The calculations of rotor loads and blade deflections were performed for periods equal to 12 revolutions of the main rotor. During the rotor, revolution the blade azimuthal positions were changed with the angle step $\Delta\psi$ equals to 5° . Data of the three-bladed rotor of light helicopter were applied for simulations. The results of the last two rotor revolutions are shown in Fig. 2 for rotor thrust, in Fig. 3 for rotor shaft moment and in Fig. 4 for blade control moment respectively.

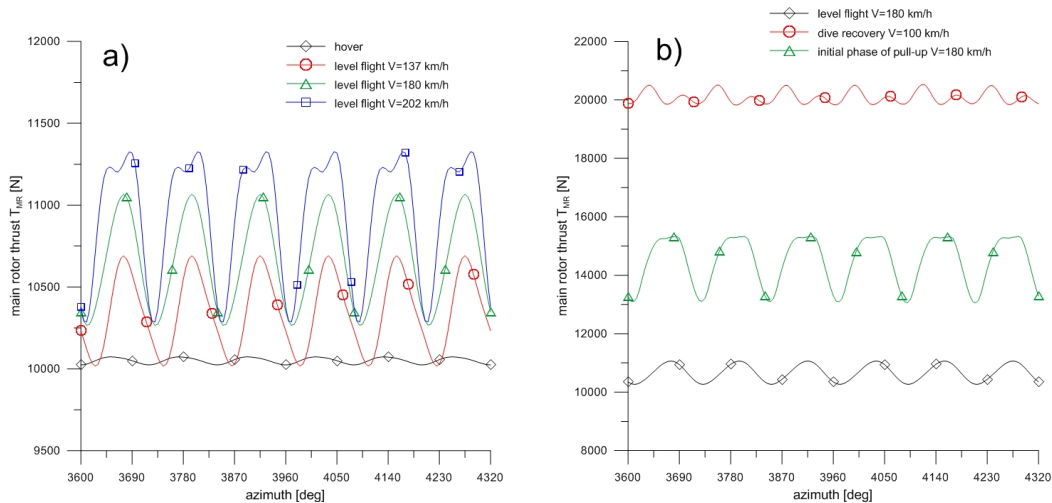


Fig. 2. Comparison of rotor thrust time-runs: a) for hover and level flights, b) for level flight, dive recovery, initial phase of pull-up

In conditions of level flights (Fig. 2a) the average value and amplitude of rotor thrust increase with flight speed. The thrust pulsations observed in hover are result of deflected swashplate position due to balance the helicopter with centre mass off-set relatively to axis of the rotor shaft. The thrust oscillations for level flight at maximum speed of 202 km/h may generate fuselage vibrations of 0.1 g magnitude. For initial phase of pull up at speed of 180 km/h, with increased blade collective pitch and cyclic pitch for pulled control stick, but for non-changed position of

fuselage with pitch angle like at level flight of 180 km/h, the thrust is enlarged over 40% (Fig. 2b) comparing to value of 180 km/h level flight. The maximum value of rotor thrust, nearly doubled comparing to level flights can be developed in dive recovery at moderate speed when fuselage nose-up pitch position reaches over 25°. In Fig. 3a can be noticed, the similar levels of torsion shaft moment for hover and maximum speed conditions, which is coincident with levels of power required for flight. At optimal flight speed of 137 km/h the observed shaft moment is at level of the half value for hover. Rather low level of the torsion shaft moment is noticed for the maximum rotor thrust condition in dive recovery (Fig. 3b) which is related with direction of airflow through the rotor disk from lower to upper area when the rotor is partly powered by airflow, similarly to autorotation.

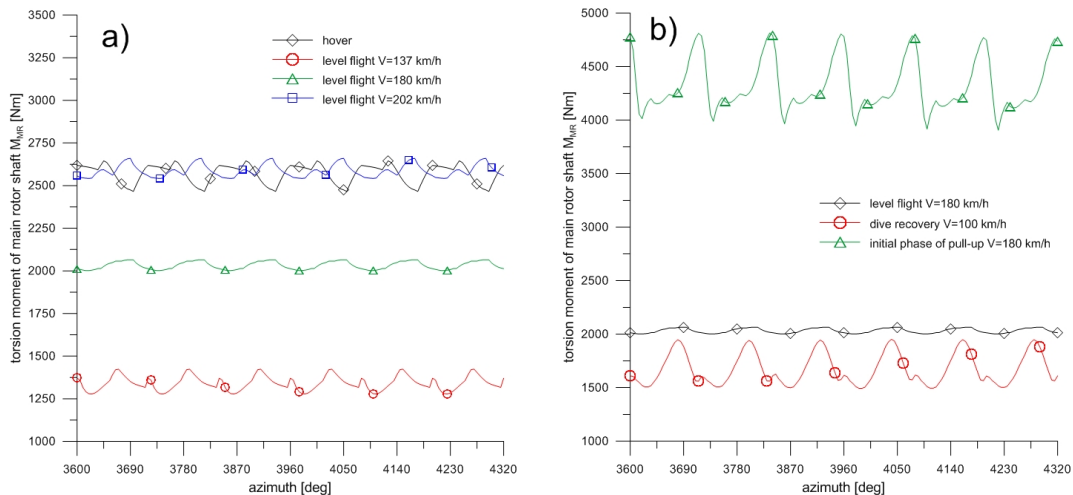


Fig. 3. Comparison of torsion moment of rotor shaft time-runs: a) for hover and level flights, b) for level flight, dive recovery, initial phase of pull-up

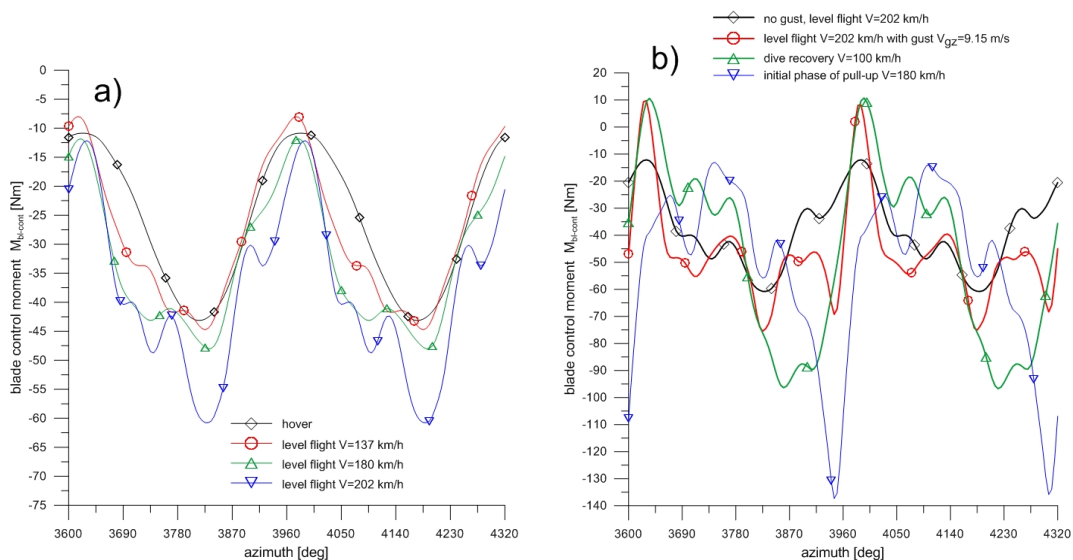


Fig. 4. Comparison of blade control moment time-runs: a) for hover and level flights, b) for level flight, wind gust, dive recovery, initial phase of pull-up

The comparison of blade control moment time-runs (Fig. 4) shows that maximum values exist at proximity of retreating blade azimuth ($3600^{\circ}+270^{\circ}$) when, due to high blade pitch angle, the aerodynamic and centrifugal forces acting on blade generate large torsion loads transmitted to helicopter control links. A significant increment of blade control moment appears in dive recovery with maximum thrust and in pull-up manoeuvre. The values of control moment exceed 100 Nm,

which may define the limits of blade pitch change rates to avoid the sharp control inputs and generation the excessive loads in rotor control system. For the higher speed flights and for manoeuvres the shapes of time-runs of blade control moments are different from sinusoidal function of blade pitch control inputs introduced by deflected swashplate. Such phenomenon can be related with increased deflections of blade especially with blade torsion deformations, which are generated in case of appearance of flow separation zones. The rotor disk distributions of blade deflections and angles of attack show the range of blade parameters changes which occur during rotor revolution for level flight at speed of 202 km/h (Fig. 5), for vertical wind gust in flight at the same speed (Fig. 6) and for pull-up manoeuvre at speed of 180 km/h (Fig. 7). In the level flight at high speed of 202 km/h the angles of torsion deformations at blade tip oscillate between -2.6° at azimuth close to 90° for advancing blade and -1.3° at azimuth 300° nearly position of retreating blade (Fig. 5a). The distribution of blade out-of-plane deflection shows forward tilt of rotor cone where blade deflection at tip reaches 0.28 m at 0° azimuth over tail boom and decreases to 0.10 m at blade azimuth position of 180° (Fig. 5b). At the region of blade tip the angle of attack values change between -2° and 10.5° (Fig. 5c) without existence of separation zone (Fig. 5d) where critical angles are greater than local attack angles.

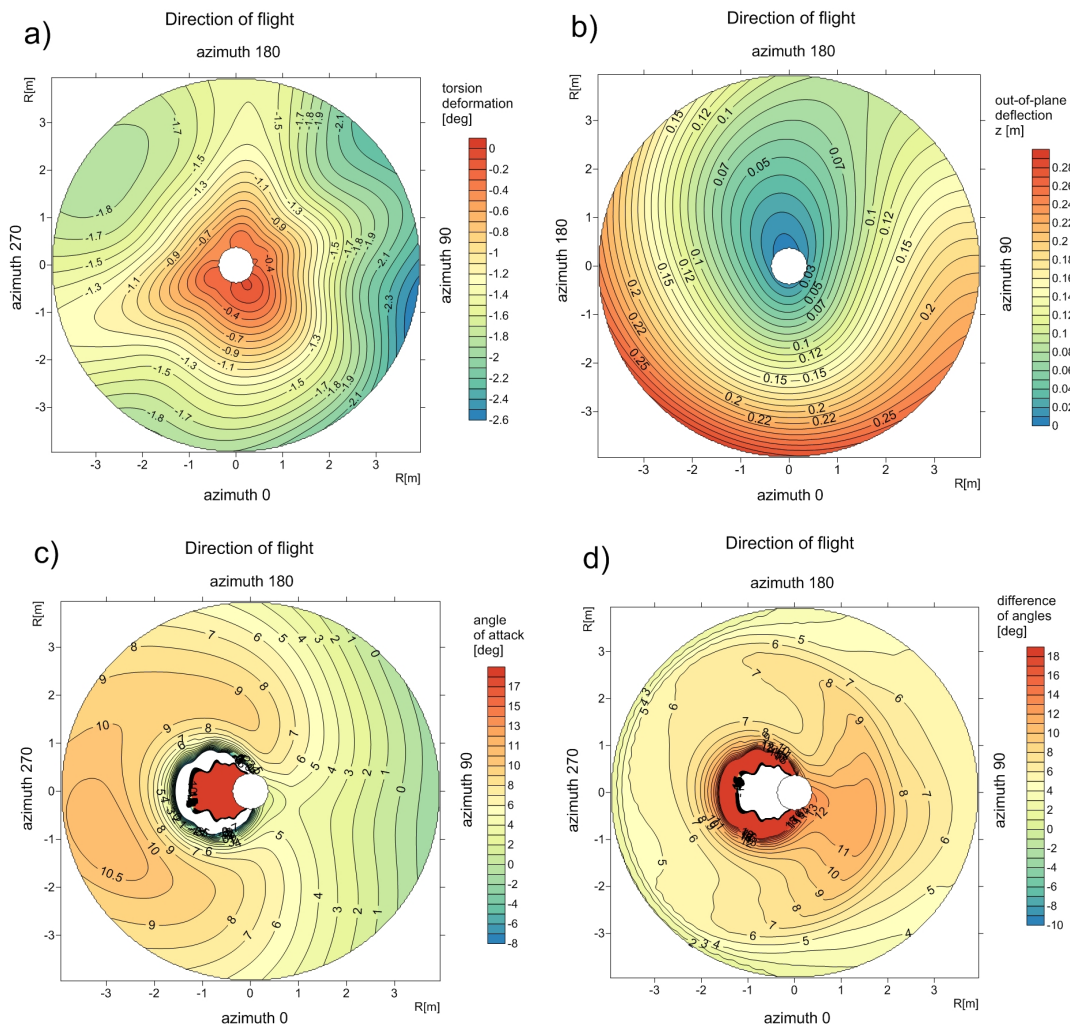


Fig. 5. Rotor disk distribution of blade parameters in level flight at velocity of 202 km/h: a) torsion blade deformation, b) out-of-plane bending deflection, c) attack angle of blade cross-sections, d) difference of critical and local attack angle of blade cross-sections

The vertical wind gust in level flight at speed of 202 km/h causes increase of attack angles (Fig. 6c) with large separation zone between azimuth of 180° and 0° . The boundary of separation

zone is shown as bold zero-isoline of difference of critical and local attack angles (Fig. 6d). In wind gust conditions the rotor blade cone is tilted backward where blade out-of-plane deflections are greater at front of rotor disk at azimuth 180° than deflections for blade at aft position at azimuth 0° (Fig. 6b). The blade passages across the boundaries of separation zones generate increased blade torsion deformations with oscillations reaching angle of -4° (Fig. 6a).

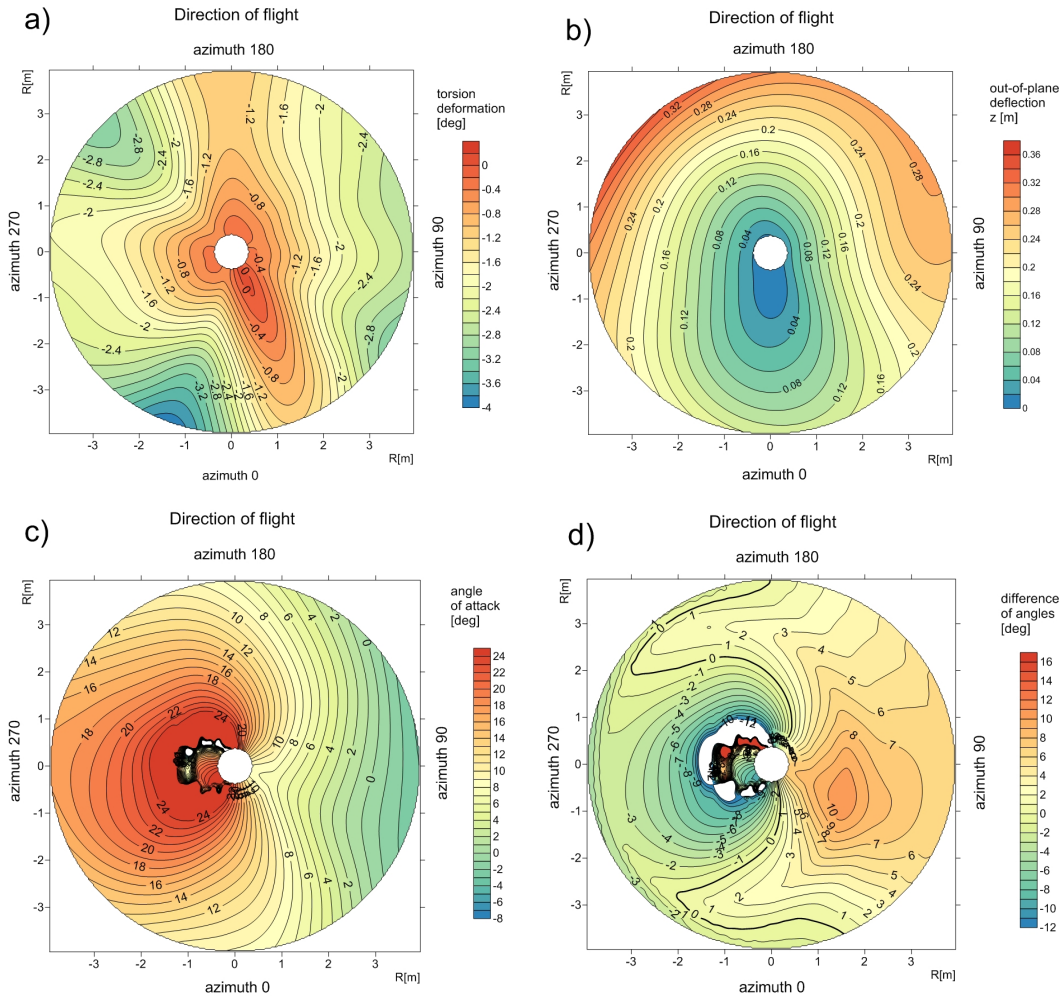


Fig. 6. Rotor disk distribution of blade parameters in level flight at velocity of 202 km/h with vertical wind gust $V_{gz} = 9.15$ m/s: a) torsion deformation, b) out-of-plane deflection, c) attack angle of blade cross-sections, d) difference of critical and local attack angle of blade cross-sections

The sharp control inputs for initial phase of pull-up in flight at speed of 180 km/h introduce greater attack angles and deeper separation zone in comparison to wind gust case (Fig. 7c, d).

The enlarged oscillations of blade torsion deformations (Fig. 7a) correspond to frequency of the first eigen mode of torsion blade vibrations. Observed in Fig. 7b distribution of blade out-of-plane deflections with high position of blade tip at azimuth of 180° shows backward tilt of rotor cone, which helps to pitch up the fuselage of helicopter. The simulation results for helicopter manoeuvres may be considered as limitations of allowed conditions of helicopter flight envelope.

4. Conclusions

Applying the simulation program, the helicopter rotor loads and behaviour of blades can be defined for states within assumed flight envelope. The results of simulation for steady flight states may help to collect data for fatigue strength determination of helicopter structure. The simulations of helicopter manoeuvres are useful for prediction the limits of safe helicopter operations.

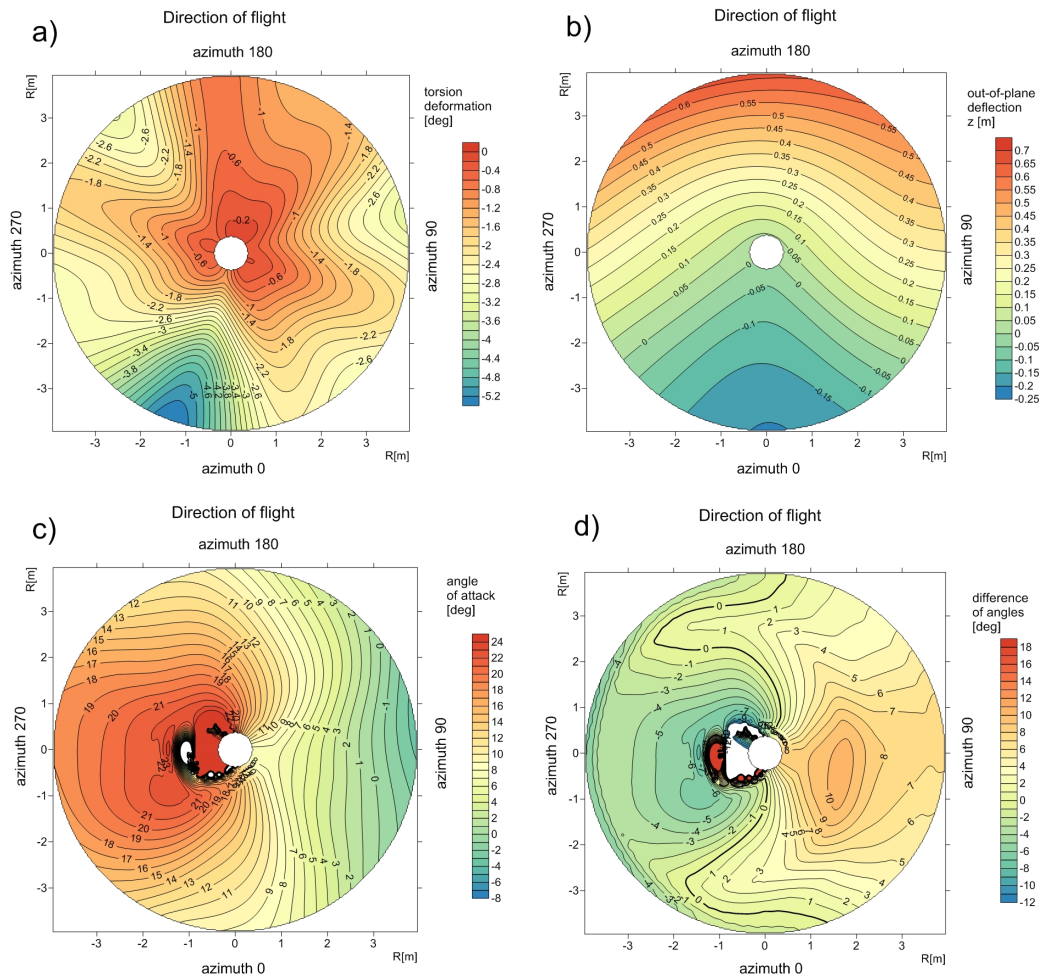


Fig. 7. Rotor disk distribution of blade parameters in the initial phase of pull-up manoeuvre at velocity of 180 km/h: a) torsion deformation, b) out-of-plane deflection, c) attack angle of blade cross-sections, d) difference of critical and local attack angle of blade cross-sections

References

- [1] Johnson, W., *Milestone in Rotorcraft Aeromechanics*, NASA/TP-2011-215971, 2011.
- [2] Bousman, W. G., Kufeld, R. M., *UH-60A Airloads Catalog*, , NASA/TM-2005-212827, 2005.
- [3] Olson, L. E., Abrego, A. I., Barrows, D. A., Burner, A. W., *Blade Deflections Measurements of a Full-Scale UH-60A Rotor System*, American Helicopter Society Aeromechanics Specialist Conference, San Francisco, California 2010.
- [4] Abrego, A. I., Meyn, L., Burner, A. W., Barrows, D. A., *Summary of Full-Scale Blade Displacement Measurements of the UH-60A Airloads Rotor*, American Helicopter Society Technical Meeting on Aeromechanics Design for Vertical Lift, San Francisco, California 2016.
- [5] Yeo, H., Johnson, W., *Comparison of Rotor Structural Loads Calculated Using Comprehensive Analysis*, 31st European Rotorcraft Forum, Florence 2005.
- [6] Biedron, R. T., Lee-Rausch, E. M., *Computation of UH-60A Airloads Using CFD/CSD Coupling on Unstructured Meshes*, American Helicopter Society 67th Annual Forum, Virginia Beach, Virginia 2011.
- [7] Gula, P., Gorecki, T., *Design, Experiments and Development of a Polish Unmanned Helicopter ILX-27*, 39st European Rotorcraft Forum, Moscow 2013.
- [8] Stanisławski, J., *Experimental measurements and simulation calculations of load in control system of helicopter*, Transactions of the Institute of Aviation, No. 1 (238), pp. 35-53, 2015.